Proceedings of ALGORITMY 2012
pp. 85–94

TWO DIMENSIONAL SIMULATION OF FLUID-STRUCTURE INTERACTION USING DGFEM

JAROSLAVA HASNEDLOVÁ-PROKOPOVÁ[†,*], MILOSLAV FEISTAUER[†], JAROMÍR HORÁČEK[*], ADAM KOSÍK[†], AND VÁCLAV KUČERA[†]

Abstract. This paper deals with the numerical simulation of the fluid-structure interaction of compressible flow with an elastic body. The work was motivated by the vibrations of human vocal folds during phonation onset. The fluid part of the problem is represented by the Navier-Stokes equations written in the ALE form. It allows us to treat the time dependence of the computational domain using the ALE (Arbitrary Lagrangian-Eulerian) method. The deformation of the elastic body is described by the linear dynamical elasticity equations. Both these system are coupled by the transmission conditions. The space-discretization of the fluid problem was carried out by the discontinuous Galerkin Finite element method (DGFEM) and for the time-discretization the backward difference formula (BDF) was used. The structural problem was discretized by the conforming finite element method and the Newmark method. The results present the applicability of the method and compare two different developed couplings.

Key words. fluid-structure interaction, compressible Navier-Stokes equations, ALE method, linear dynamical elasticity equations, coupling procedure

AMS subject classifications. 15A15, 15A09, 15A23

1. Introduction. At the current speed of technological progress, the coupled problems describing the interactions of fluid flow with elastic structure motion are of great importance in many fields of physical and technical sciences such as biomechanics, aerospace, civil and mechanical engineering, etc. In our work we are inspired by the flow-induced vibrations in the human vocal folds. In current publications various simplified glottal flow models are used. They are based on the Bernoulli equation ([1]), 1D models for an incompressible inviscid fluid ([2]), 2D incompressible Navier-Stokes equations solved by the finite volume method ([3]) or finite element method ([4]). From the papers dealing with the compressible Navier-Stokes equations we can mention [5], where the finite volume method is used and the motion of the channel cross-section of the glottal channel is prescribed. Our aim is the finite element model of the fluid-structure interaction of the viscous compressible flow with the elastic body.

2. Continuous problem. This section is devoted to the formulation of the interaction problem. We treat the compressible flow and the elasticity of the body separately.

2.1. Formulation of the flow problem. We are concerned with the problem of compressible flow in a time-dependent bounded domain $\Omega_t \subset \mathbb{R}^2$ with $t \in [0, T]$. The boundary of Ω_t is formed by three disjoint parts: $\partial\Omega_t = \Gamma_I \cup \Gamma_O \cup \Gamma_{W_t}$, where Γ_I is the inlet, Γ_O is the outlet and Γ_{W_t} represents impermeable time-dependent walls.

The time dependence of the domain Ω_t is taken into account with the aid of the *Arbitrary Lagrangian-Eulerian* (ALE) method, see e.g. [6]. The basis of this approach is created by a regular one-to-one ALE mapping of the reference configuration Ω_0 onto

[*]Institute of Thermomechanics, Academy of Sciences of the Czech Republic, v.v.i., Dolejškova 1402/5, 182 00 Praha 8 (corresponding author's email: jarkaprokop@post.cz).
[†]Charles University, Faculty of Mathematics and Physics, Sokolovská 83, 18675 Praha 8.

the current configuration Ω_t :

$$\mathcal{A}_t : \bar{\Omega}_0 \longrightarrow \bar{\Omega}_t, \ i.e. \ \boldsymbol{X} \in \bar{\Omega}_0 \longmapsto \boldsymbol{x} = \boldsymbol{x}(\boldsymbol{X}, t) = \mathcal{A}_t(\boldsymbol{X}) \in \bar{\Omega}_t.$$

Further, we define the domain velocity:

$$\begin{aligned} \tilde{\boldsymbol{z}}(\boldsymbol{X}, t) &= \frac{\partial}{\partial t}\mathcal{A}_t, \quad t \in [0, T], \ \boldsymbol{X} \in \Omega_0, \\ \boldsymbol{z}(\boldsymbol{x}, t) &= \tilde{\boldsymbol{z}}(\mathcal{A}_t^{-1}(\boldsymbol{x}), t), \ t \in [0, T], \ \boldsymbol{x} \in \Omega_t \end{aligned} \tag{2.1}$$

and the ALE derivative of the state vector function $\boldsymbol{w} = \boldsymbol{w}(\boldsymbol{x}, t)$ defined for $\boldsymbol{x} \in \Omega_t$ and $t \in [0, T]$:

$$\begin{aligned} \frac{D^{\mathcal{A}}}{Dt}\boldsymbol{w}(\boldsymbol{x}, t) &= \frac{\partial \tilde{\boldsymbol{w}}}{\partial t}(\boldsymbol{X}, t), \\ \tilde{\boldsymbol{w}}(\boldsymbol{X}, t) = \boldsymbol{w}(\mathcal{A}_t(\boldsymbol{X}), t), \ \boldsymbol{X} \in \Omega_0, \ \boldsymbol{x} = \mathcal{A}_t(\boldsymbol{X}, t), \ \boldsymbol{X} \in \Omega_0, \ \boldsymbol{x} = \mathcal{A}_t(X). \end{aligned} \tag{2.2}$$

Using the chain rule we are able to express the ALE derivative in the form

$$\frac{D^{\mathcal{A}} w_i}{Dt} = \frac{\partial w_i}{\partial t} + \mathrm{div}(\boldsymbol{z} w_i) - w_i \mathrm{div}\boldsymbol{z}, \quad i = 1, \ldots, 4. \tag{2.3}$$

Application of (2.3) to the continuity equation, the Navier-Stokes equations and the energy equation leads to the governing system in the ALE form

$$\frac{D^{\mathcal{A}}\boldsymbol{w}}{Dt} + \sum_{s=1}^{2} \frac{\partial \boldsymbol{g}_s(\boldsymbol{w})}{\partial x_s} + \boldsymbol{w}\mathrm{div}\boldsymbol{z} = \sum_{s=1}^{2} \frac{\partial \boldsymbol{R}_s(\boldsymbol{w}, \nabla \boldsymbol{w})}{\partial x_s}, \tag{2.4}$$

where

$$\begin{aligned} \boldsymbol{w} &= (\rho, \rho v_1, \rho v_2, E)^T \in I\!R^4, \\ \boldsymbol{g}_s(\boldsymbol{w}) &= \boldsymbol{f}_s - z_s \boldsymbol{w}, \ s = 1, 2, \\ \boldsymbol{f}_s &= (\rho v_s, \rho v_1 v_s + \delta_{1s} p, \rho v_2 v_s + \delta_{2s} p, (E + p) v_s)^T, \ s = 1, 2, \\ \boldsymbol{R}_s(\boldsymbol{w}, \nabla \boldsymbol{w}) &= (0, \tau_{s1}^V, \tau_{s2}^V, \tau_{s1}^V v_1 + \tau_{s2}^V v_2 + k\frac{\partial \theta}{\partial x_s})^T, \ s = 1, 2, \\ \tau_{ij}^V &= \lambda \delta_{ij} \mathrm{div}\boldsymbol{v} + 2\mu d_{ij}(\boldsymbol{v}), \ d_{ij}(\boldsymbol{v}) = \frac{1}{2}\left(\frac{\partial v_i}{\partial x_j} + \frac{\partial v_j}{\partial x_i}\right), \ i, j = 1, 2. \end{aligned}$$

For a detailed description see, for example, [7]. The following notation is used: ρ – fluid density, p – pressure, E – total energy, $\boldsymbol{v} = (v_1, v_2)$ – velocity vector, θ – absolute temperature, $c_v > 0$ – specific heat at constant volume, $\gamma > 1$ – Poisson adiabatic constant, $\mu > 0, \lambda = -2\mu/3$ – viscosity coefficients, $k > 0$ – heat conduction coefficient, τ_{ij}^V – components of the viscous part of the stress tensor. The vector-valued function $\boldsymbol{w}$ is called the state vector, $\boldsymbol{f}_s$ are inviscid fluxes and $\boldsymbol{R}_s$ represent viscous terms. The system (2.4) is completed by the thermodynamical relations

$$p = (\gamma - 1)\left(E - \rho\frac{|\boldsymbol{v}|^2}{2}\right), \quad \theta = \frac{1}{c_v}\left(\frac{E}{\rho} - \frac{1}{2}|\boldsymbol{v}|^2\right) \tag{2.5}$$

and equipped with the initial condition

$$\boldsymbol{w}(\boldsymbol{x}, 0) = \boldsymbol{w}^0(\boldsymbol{x}), \ \boldsymbol{x} \in \Omega_0 \tag{2.6}$$

and the boundary conditions

$$\begin{aligned}
&\text{Inlet } \Gamma_I: \quad \rho = \rho_D, \quad \boldsymbol{v} = \boldsymbol{v}_D = (v_{D1}, v_{D2}), \quad \sum_{j=1}^{2}\left(\sum_{i=1}^{2}\tau_{ij}^V n_i\right) v_j + k\frac{\partial\theta}{\partial \boldsymbol{n}} = 0,\\
&\text{Moving wall } \Gamma_{W_t}: \quad \boldsymbol{v} = \boldsymbol{z}_D(t) = \text{velocity of a moving wall}, \quad \frac{\partial\theta}{\partial \boldsymbol{n}} = 0, \qquad (2.7)\\
&\text{Outlet } \Gamma_O: \quad \sum_{j=1}^{2}\tau_{ij}^V n_j = 0, \quad \frac{\partial\theta}{\partial \boldsymbol{n}} = 0, \quad i = 1,2,
\end{aligned}$$

with prescribed data $\rho_D,\ \boldsymbol{v}_D,\ \boldsymbol{z}_D$. By $\boldsymbol{n}$ we denote the unit outer normal.

2.2. Elasticity problem. Let us have a bounded open set $\Omega^b \subset I\!R^2$ representing an elastic body, which has a common boundary with the reference domain Ω_0 occupied by the fluid at the initial time. Further, the boundary of Ω^b is formed by two disjoint parts $\partial\Omega^b = \Gamma_W^b \cup \Gamma_D^b$, where $\Gamma_W^b \cap \Gamma_D^b = \emptyset$, $\Gamma_W^b \subset \Gamma_{W_0}$ and Γ_D^b is a fixed part of the boundary. Using the notation of the displacement of the body $\boldsymbol{u}(\boldsymbol{X},t) = (u_1(\boldsymbol{X},t), u_2(\boldsymbol{X},t))$, $\boldsymbol{X} = (X_1, X_2) \in \Omega^b$, $t \in (0,T)$ we can write the equations describing the deformation of the elastic body Ω^b in the form

$$\rho^b\frac{\partial^2 u_i}{\partial t^2} + C\rho^b\frac{\partial u_i}{\partial t} - \sum_{j=1}^{2}\frac{\partial\tau_{ij}^b}{\partial X_j} = 0 \quad \text{in } \Omega^b\times(0,T),\ i = 1,2. \qquad (2.8)$$

Here $(\tau_{ij}^b)_{i,j=2}^2$ represents the stress tensor fulfilling the generalized Hooke's law for an isotropic material

$$\tau_{ij}^b = \tilde{\lambda}\mathrm{div}\boldsymbol{u}\delta_{ij} + 2\tilde{\mu}e_{ij}, \quad i,j = 1,2, \qquad (2.9)$$

where $(e_{ij})_{i,j=2}^2$ is the strain tensor with the components

$$e_{ij} = \frac{1}{2}\left(\frac{\partial u_i}{\partial X_j} + \frac{\partial u_j}{\partial X_i}\right), \quad i,j = 1,2 \qquad (2.10)$$

and ρ^b is the density of the solid material. The Lamé coefficients are denoted by $\tilde{\lambda},\ \tilde{\mu}$ and are used in the definition of the Young modulus E^b and Poisson ratio σ^b :

$$E^b = \frac{\tilde{\mu}(3\tilde{\lambda}+2\tilde{\mu})}{\tilde{\lambda}+\tilde{\mu}}, \quad \sigma^b = \frac{\tilde{\lambda}}{2(\tilde{\lambda}+\tilde{\mu})}. \qquad (2.11)$$

The dissipation of the energy of the system is represented by the expression $C\rho^b\frac{\partial u_i}{\partial t}$, where $C \in I\!R$ and $C \geq 0$. The formulation of the dynamical elasticity problem (2.8) is completed by the initial conditions

$$\boldsymbol{u}(\boldsymbol{X},0) = 0 \text{ and } \frac{\partial\boldsymbol{u}}{\partial t}(\boldsymbol{X},0) = 0\ \boldsymbol{X} \in \Omega^b \qquad (2.12)$$

and boundary conditions:

$$\sum_{j=1}^{2}\tau_{ij}^b n_j = T_i^{\boldsymbol{n}} \quad \text{on } \Gamma_W^b\times(0,T), \quad i = 1,2, \qquad (2.13)$$

$$\boldsymbol{u} = 0 \quad \text{on } \Gamma_D^b\times(0,T). \qquad (2.14)$$

The components of the normal stress are denoted by $T_i^n,\ i = 1,2$.

2.3. Fluid-structure interaction coupling and the ALE mapping. The common boundary $\tilde{\Gamma}_{W_t}$ between the fluid and the structure at time t, is given by

$$\tilde{\Gamma}_{W_t} = \left\{ \boldsymbol{x} \in I\!R^2;\ \boldsymbol{x} = \boldsymbol{X} + \boldsymbol{u}(\boldsymbol{X}, t),\ \boldsymbol{X} \in \Gamma_W^b \right\}. \tag{2.15}$$

This means that the domain Ω_t is determined by the displacement $\boldsymbol{u}$ of the part Γ_W^b at time t. If we know the domain Ω_t occupied by the fluid at time t, the flow problem can be solved and the surface force acting on the body on $\tilde{\Gamma}_{W_t}$ can be determined. Then the transformation of the surface force to the reference configuration, i.e. to the interface Γ_W^b is realized. In the case of the linear elasticity model, when only small deformations are considered, we get the transmission condition

$$\sum_{j=1}^{2} \tau_{ij}^b(\boldsymbol{X}) n_j(\boldsymbol{X}) = -\sum_{j=1}^{2} \tau_{ij}^f(\boldsymbol{x}) n_j(\boldsymbol{X}), \quad i,j = 1,2, \tag{2.16}$$

where τ_{ij}^f are the components of the stress tensor of the fluid

$$\tau_{ij}^f = -p\delta_{ij} + \tau_{ij}^V,\ i,j = 1,2 \tag{2.17}$$

and points $\boldsymbol{x}$ and $\boldsymbol{X}$ satisfy the relation

$$\boldsymbol{x} = \boldsymbol{X} + \boldsymbol{u}(\boldsymbol{X}, t). \tag{2.18}$$

By $\boldsymbol{n}(\boldsymbol{X}) = (n_1(\boldsymbol{X}), n_2(\boldsymbol{X}))$ we denote the unit outer normal to the body Ω^b on Γ_W^b at the point $\boldsymbol{X}$. Further, the fluid velocity is defined on the moving part of the boundary Γ_{W_t} by the transmission condition

$$\boldsymbol{v}(\boldsymbol{x}, t) = \boldsymbol{z}_D(\boldsymbol{x}, t) = \frac{\boldsymbol{u}(\boldsymbol{X}, t)}{\partial t}. \tag{2.19}$$

The ALE mapping $\mathcal{A}_t$ is determined with the aid of an artificial stationary elasticity problem, where we seek $\boldsymbol{d} = (d_1, d_2)$ defined in Ω_0 as a solution of the elastic system

$$\sum_{j=1}^{2} \frac{\partial \tau_{ij}^a}{\partial x_j} = 0 \quad \text{in } \Omega_0, \quad i = 1,2, \tag{2.20}$$

where τ_{ij}^a are the components of the artificial stress tensor

$$\tau_{ij}^a = \lambda^a \mathrm{div}\boldsymbol{d}\delta_{ij} + 2\mu^a e_{ij}^a(\boldsymbol{d}), \quad e_{ij}^a(\boldsymbol{d}) = \frac{1}{2}\left(\frac{\partial d_i}{\partial x_j} + \frac{\partial d_j}{\partial x_i} \right), \quad i,j = 1,2. \tag{2.21}$$

The artificial Young modulus E^a and the artificial Poisson ratio σ^a can be derived from Lamé coefficients λ^a and μ^a in the same way as in (2.11). The problem is again completed by the boundary conditions:

$$\boldsymbol{d}|_{\Gamma_I \cup \Gamma_O} = 0,\ \boldsymbol{d}|_{\Gamma_{W_0} \setminus \Gamma_W^b} = 0,\ \boldsymbol{d}(\boldsymbol{x}, t) = \boldsymbol{u}(\boldsymbol{x}, t),\ \boldsymbol{x} \in \Gamma_W^b. \tag{2.22}$$

The solution of the problem (2.20) – (2.22) gives us the ALE mapping of $\bar{\Omega}_0$ onto $\bar{\Omega}_t$ in the form

$$\mathcal{A}_t(\boldsymbol{x}) = \boldsymbol{x} + \boldsymbol{d}(\boldsymbol{x}, t), \quad \boldsymbol{x} \in \bar{\Omega}_0, \tag{2.23}$$

for each time t.

Based on the above mentioned ideas we can formulate the continuous FSI problem: Our aim is to determine the domain $\Omega_t,\ t \in (0,T]$ and function $\boldsymbol{w} = \boldsymbol{w}(\boldsymbol{x},t),\ \boldsymbol{x} \in \bar{\Omega}_t,\ t \in [0,T]$ and $\boldsymbol{u} = \boldsymbol{u}(\boldsymbol{X},t),\ \boldsymbol{X} \in \bar{\Omega}^b,\ t \in [0,T]$ satisfying equations (2.4), (2.8), the initial conditions (2.6), (2.12), the boundary conditions (2.7), (2.13),(2.14) and the transmission conditions (2.16), (2.19).

3. Discrete problem. The described FSI problem represents a strongly nonlinear dynamical system, where the theoretical analysis of the qualitative properties of this problem is open. Therefore, we shall be concerned with its numerical solution. In the following we describe numerical methods for the solution of separately considered flow and structural problems and the construction of the ALE mapping.

3.1. Discretization of the flow problem. For the space semidiscretization we use the discontinuous Galerkin finite element method (DGFEM).

We construct a polygonal approximation Ω_{ht} of the domain Ω_t. By $\mathcal{T}_{ht}$ we denote a partition of the closure $\bar{\Omega}_{ht}$ of the domain Ω_{ht} into a finite number of closed triangles K with mutually disjoint interiors such that $\bar{\Omega}_{ht} = \bigcup_{K\in\mathcal{T}_{ht}} K$. The approximate solution will be sought in the space of piecewise polynomial functions

$$\boldsymbol{S}_{ht} = [S_{ht}]^4, \quad \text{with } S_{ht} = \{v; v|_K \in P_r(K)\ \forall\, K \in \mathcal{T}_{ht}\}, \tag{3.1}$$

where $r \geq 0$ is an integer and $P_r(K)$ denotes the space of all polynomials on K of degree $\leq r$. A function $\boldsymbol{\varphi} \in \boldsymbol{S}_{ht}$ is, in general, discontinuous on interior edges of the triangulation.

The discrete problem is derived in the following way: We multiply system (2.4) by a test function $\boldsymbol{\varphi}_h \in \boldsymbol{S}_{ht}$, integrate over $K \in \mathcal{T}_{ht}$, apply Green's theorem, sum over all elements $K \in \mathcal{T}_{ht}$, use the concept of the numerical flux and introduce suitable terms mutually cancelling for a regular exact solution. Moreover, we carry out a linearization of the nonlinear terms. Then, the semidiscrete solution of problem (2.4) is defined as a function $\boldsymbol{w}_h \in C^1((0,T), \boldsymbol{S}_{ht})$ fulfilling the conditions

$$\begin{aligned}&\left(\frac{D^{\mathcal{A}}\boldsymbol{w}_h}{Dt}(t), \boldsymbol{\varphi}_h\right) + d_h(\boldsymbol{w}_h(t), \boldsymbol{\varphi}_h) + b_h(\boldsymbol{w}_h(t), \boldsymbol{\varphi}_h) \qquad (3.2)\\ &+a_h(\boldsymbol{w}_h(t), \boldsymbol{\varphi}_h) + J_h(\boldsymbol{w}_h(t), \boldsymbol{\varphi}_h) = l_h(\boldsymbol{w}_h(t), \boldsymbol{\varphi}_h) \quad \forall \boldsymbol{\varphi}_h \in \boldsymbol{S}_{ht},\ \forall t \in (0,T),\\ &\boldsymbol{w}_h(0) = \boldsymbol{w}_h^0, \qquad (3.3)\end{aligned}$$

where $\boldsymbol{w}_h^0$ is $L^2(\Omega_{h0})$-projection of $\boldsymbol{w}^0$ on $\boldsymbol{S}_{h0}$. This means that

$$\left(\boldsymbol{w}_h^0, \boldsymbol{\varphi}_h\right) = \left(\boldsymbol{w}^0, \boldsymbol{\varphi}_h\right) \quad \forall \boldsymbol{\varphi}_h \in \boldsymbol{S}_{h0}. \tag{3.4}$$

For a detailed description of the whole process see [7].

In the case of the time discretization of (3.2) we construct a partition $0 = t_0 < t_1 < t_2 \ldots$ of the time interval $[0,T]$ and define the time step $\tau_k = t_{k+1} - t_k$. We use the approximations $\boldsymbol{w}_h(t_n) \approx \boldsymbol{w}_h^n \in \boldsymbol{S}_{ht_n},\ \boldsymbol{z}(t_n) \approx \boldsymbol{z}^n,\ n = 0,1,\ldots$ and introduce the function $\hat{\boldsymbol{w}}_h^k = \boldsymbol{w}_h^k \circ \mathcal{A}_{t_k} \circ \mathcal{A}_{t_{k+1}}^{-1}$, which is defined in the domain $\Omega_{ht_{k+1}}$. The ALE derivative at time t_{k+1} is approximated by the first-order backward finite difference

$$\frac{D^A\boldsymbol{w}_h}{Dt}(\boldsymbol{x}, t_{k+1}) \approx \frac{\boldsymbol{w}_h^{k+1}(\boldsymbol{x}) - \hat{\boldsymbol{w}}_h^k(\boldsymbol{x})}{\tau_k}. \tag{3.5}$$

The remaining terms are treated with the aid of a linearization and extrapolation. For details see [7].

3.2. Discretization of the structural problem. The space semidiscretization of the structural problem is carried out by the conforming finite element method. By Ω_h^b we denote a polygonal approximation of the domain Ω^b. We construct a triangulation $\mathcal{T}_h^b$ of the domain Ω_h^b formed by a finite number of closed triangles. Then the approximate solution of the structural problem is sought in the finite-dimensional space $\boldsymbol{X}_h = X_h \times X_h$, where

$$X_h = \left\{ v_h \in C(\bar{\Omega}_h^b);\ v_h|_K \in P^s(K),\ \forall K \in \mathcal{T}_h^b \right\}. \tag{3.6}$$

Here $s \geq 1$ is an integer. In $\boldsymbol{X}_h$ we define the subspace $\boldsymbol{V}_h = V_h \times V_h$, where

$$V_h = \left\{ y_h \in X_h; y_h|_{\bar{\Gamma}_{Dh}^b} = 0 \right\}. \tag{3.7}$$

The derivation of the space semidiscretization can be obtained in a standard way. Multiplying system (2.8) by any test function $y_{hi} \in V_h,\ i = 1, 2$, applying Green's theorem and using the boundary condition (2.13). Using the notation $\boldsymbol{u}_h'(t) = \frac{\partial \boldsymbol{u}_h(t)}{\partial t}$ and $\boldsymbol{u}_h''(t) = \frac{\partial^2 \boldsymbol{u}_h(t)}{\partial t^2}$ we define the approximate solution of the structural problem as a function $t \in [0, T] \to \boldsymbol{u}_h(t) \in \boldsymbol{V}_h$ such that there exist the derivatives $\boldsymbol{u}_h'(t)$, $\boldsymbol{u}_h''(t)$ and the identity

$$(\rho^b \boldsymbol{u}_h''(t), \boldsymbol{y}_h)_{\Omega_h^b} + (C\rho^b \boldsymbol{u}_h'(t), \boldsymbol{y}_h)_{\Omega_h^b} + a(\boldsymbol{u}_h(t), \boldsymbol{y}_h) = (\boldsymbol{T}_h^{\boldsymbol{n}}(t), \boldsymbol{y}_h)_{\Gamma_{Wh}}, \tag{3.8}$$
$$\forall \boldsymbol{y}_h \in \boldsymbol{V}_h, \quad \forall t \in (0, T),$$

and the initial conditions

$$\boldsymbol{u}_h(\boldsymbol{X}, 0) = 0, \quad \boldsymbol{u}_h'(\boldsymbol{X}, 0) = 0, \quad \boldsymbol{X} \in \Omega_h^b. \tag{3.9}$$

are satisfied. This approach leads to a system of ordinary differential equations. The time discretization is carried out by the Newmark method. For details see [8].

3.3. Construction of the ALE mapping. System (2.20) is discretized by conforming piecewise linear finite elements on the mesh $\mathcal{T}_{h0}$ used for computing the flow field at the beginning of the computational process in the polygonal approximation Ω_{h0} of the domain Ω_0. The use of linear finite elements is sufficient, because we need only to know the movement of the vertices of the mesh.

4. Coupling procedure. In the solution of the complete coupled fluid-structure interaction problem it is necessary to apply a suitable coupling procedure. The general framework can be found, e.g. in [9]. In our case we apply two different types of algorithms.

First, we present the *weak coupling* algorithm:

1. Compute the approximate solution of the flow problem (2.4) on the time level t_m.
2. Compute the stress tensor of the fluid τ_{ij}^f and the aerodynamical force acting on the structure and transform it to the interface Γ_{Wh}^b by (2.16).
3. Solve the elasticity problem (2.8), compute the deformation $\boldsymbol{u}_{h,m}$ at time t_m and approximate the domain $\Omega_{ht_{m+1}}$.
4. Determine the ALE mapping $\mathcal{A}_{t_{m+1}h}$ by (2.20) and approximate the domain velocity $\boldsymbol{z}_{h,m+1}$ by (2.19).
5. Set $m := m + 1$, go to 1).

The *strong coupling* procedure represents a more complicated coupling algorithm. It follows this outline:

1. Assume that the approximate solution $\boldsymbol{w}_h^m$ of the flow problem and the deformation $\boldsymbol{u}_{h,m}$ of the structure are known on the time level t_m.
2. Set $\boldsymbol{u}_{h,m+1}^0 := \boldsymbol{u}_{h,m},\ k := 1$ and apply the iterative process:
   (a) Compute the stress tensor of the fluid τ_{ij}^f and the aerodynamical force acting on the structure and transform it to the interface Γ_{Wh}^b.
   (b) Solve the elasticity problem, compute the approximation of the deformation $\boldsymbol{u}_{h,m+1}^k$ and construct the approximation $\Omega_{ht_{m+1}}^k$ of the flow domain at time t_{m+1}.
   (c) Determine the approximations of ALE mapping $\mathcal{A}_{t_{m+1}h}^k$ and the domain velocity $\boldsymbol{z}_{h,m+1}^k$.
   (d) Solve the flow problem in $\Omega_{ht_{m+1}}^k$ and obtain the approximate solution $\boldsymbol{w}_{h,m+1}^k$.
   (e) If the variation of the displacement $\boldsymbol{u}_{h,m+1}^k$ and $\boldsymbol{u}_{h,m+1}^{k-1}$ is larger than the prescribed tolerance, go to a) and $k := k+1$. Else $\Omega_{ht_{m+1}} := \Omega_{ht_m}^k,\ \boldsymbol{w}_h^{m+1} := \boldsymbol{w}_{h,m+1}^k,\ \boldsymbol{u}_h^{m+1} := \boldsymbol{u}_{h,m}^k,\ m := m+1$ and goto 2).

The difference between these two coupling algorithms will be presented on our numerical results in Section 5.

5. Numerical results. We consider the model of flow through a channel with two bumps which represent time dependent boundaries between the flow and a simplified model of vocal folds (see Figure 5.1). The numerical experiments were carried

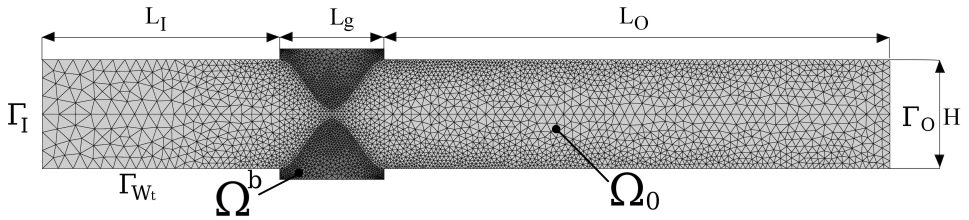

FIG. 5.1. *Computational domain at time $t = 0$ with a finite element mesh and the description of its size: $L_I = 50\,mm$, $L_g = 15.4\,mm$, $L_O = 94.6\,mm$, $H = 16\,mm$. The width of the channel in the narrowest part is $1.6\,mm$.*

out for the following data: magnitude of the inlet velocity $v_{in} = 4$ m/s, the viscosity $\mu = 15 \cdot 10^{-6}\ \mathrm{kg\,m^{-1}\,s^{-1}}$, the inlet density $\rho_{in} = 1.225\ \mathrm{kg\,m^{-3}}$, the outlet pressure $p_{out} = 97611$ Pa, the Reynolds number $Re = \rho_{in} v_{in} H/\mu = 5227$, heat conduction coefficient $k = 2.428 \cdot 10^{-2}\,\mathrm{kg\,m\,s^{-2}\,K^{-1}}$, the specific heat $c_v = 721.428\,\mathrm{m^2\,s^{-2}\,K^{-1}}$, the Poisson adiabatic constant $\gamma = 1.4$. The inlet Mach number is $M_{in} = 0.012$. The Young modulus and the Poisson ratio have values $E^b = 25000$ Pa and $\sigma^b = 0.4$, respectively, the structural damping coefficient is equal to the constant $C = 100\ \mathrm{s^{-1}}$ and the material density $\rho^b = 1040\,\mathrm{kg\,m^{-3}}$.

In the numerical experiments quadratic ($r = 2$) and linear ($s = 1$) elements were used for the approximation of the flow and structural problem, respectively.

In Table 5.1 we characterize the computational meshes used by the number of elements in the flow part and in the structure part of the mesh. Figure 5.1 shows the situation at the initial time $t = 0$ corresponding to the computational mesh 1. In Figure 5.2 we see the positions of sensor points used in the analysis.

First we tested the influence of the density of the computational meshes on the oscillations of the pressure averaged over the outlet Γ_O and the corresponding Fourier

Mesh	Colour used in graphs	Flow part	Structure part
Mesh 1	red	5398	1998
Mesh 2	green	10130	2806
Mesh 3	blue	20484	4076

TABLE 5.1
Computational meshes.

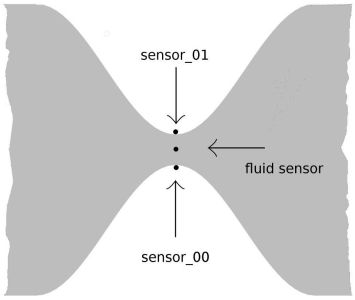

FIG. 5.2. *Positions of some sensors in the narrowest part of the channel used in the analysis*

analysis. The time step used in the compared computations was $4 \cdot 10^{-7}$s. Figure 5.3 shows the behaviour of the quantity

$$p_{av}(t) = \int_{\Gamma_O} \left(p(\boldsymbol{x}, t) - \frac{1}{T} \int_0^T p(\boldsymbol{x}, t) \mathrm{d}t \right) \mathrm{d}S / \int_{\Gamma_O} \mathrm{d}S \tag{5.1}$$

in dependence on time, computed with the aid of the strong coupling (left) and the weak coupling (right). Figure 5.4 shows the corresponding Fourier analysis. During successive mesh refinement one can observe the convergence tendency manifested by the decrease of the magnitude of the quantity p_{av} fluctuations and the decrease of the magnitude of the Fourier spectra.

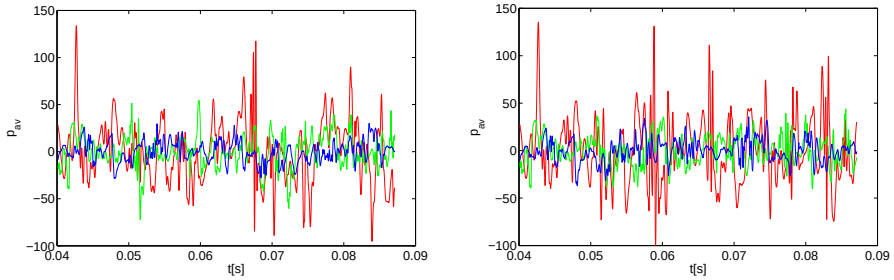

FIG. 5.3. *Dependence of the quantity p_{av} computed on three meshes: strong coupling (left), weak coupling (right).*

In order to compare the impact of the used coupling procedure we present graphs of the quantity p_{av} on the different meshes computed by the strong coupling (blue) and the weak coupling (red). Figure 5.5 shows that the difference between the results obtained by the strong and weak coupling is not too large. The same fact can be

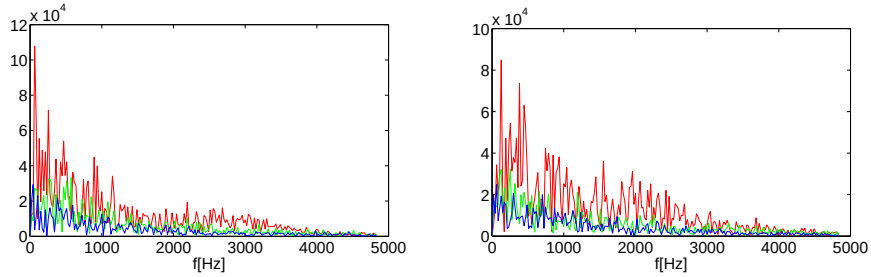

FIG. 5.4. *Fourier analysis of the quantity p_{av} computed on three meshes: strong coupling (left), weak coupling (right).*

observed in Figures 5.3 and 5.4. The main difference is in the higher stability of the strong coupling during solution the problem on a long time interval. On the other hand, the strong coupling requires naturally longer CPU time.

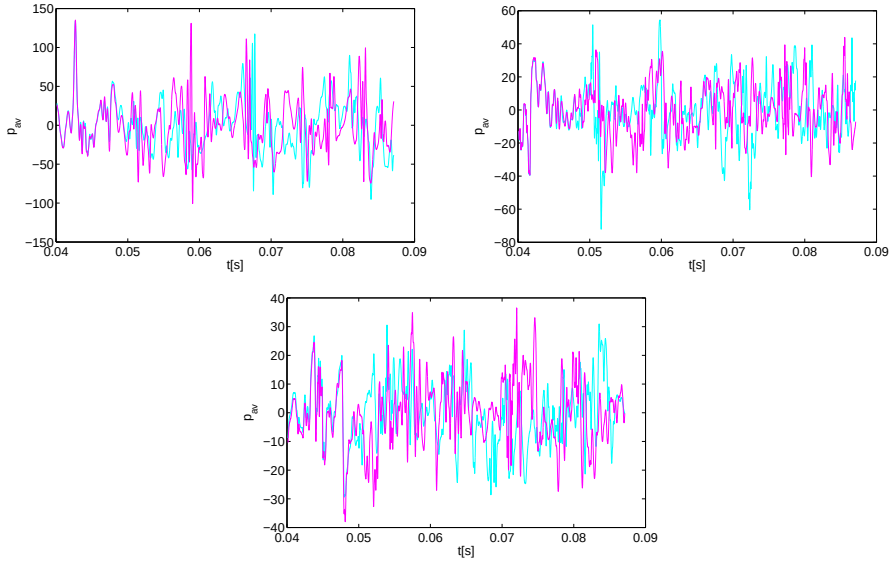

FIG. 5.5. *Comparison of the weak coupling (red) and the strong coupling (blue) on the meshes 1, 2 and 3.*

The character of the vocal folds vibration can be indicated in Figure 5.6, which shows the displacements of the sensor points on the vocal folds surface (marked in Figure 5.2) and the fluid pressure fluctuations in the middle of the gap.

6. Conclusion. A robust higher-order method for the numerical simulation of the interaction of compressible flow with elastic structures has been presented. The numerical tests show the convergence tendency of this method during successive mesh refinement and the good applicability of the method for the numerical solution of the simplified models of phonation onset. Unfortunatelly, we are not able to treat the complete closure of the channel due to the degeneration of the computational mesh. This remains as the next step of our implementation.

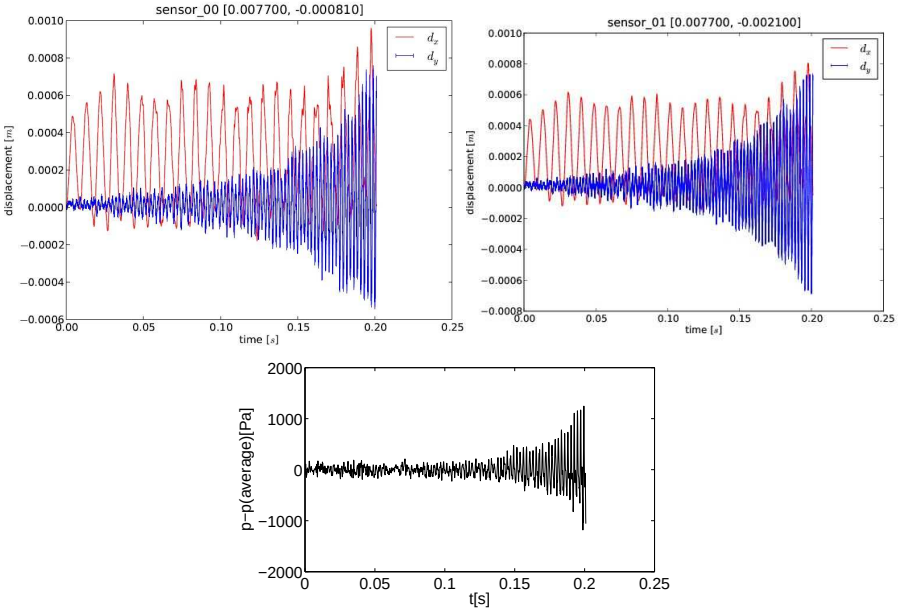

FIG. 5.6. *Displacement of the structure and the pressure of the fluid in the marked sensor points. (The computation were carried out using the mesh 2.)*

Acknowledgments. This work was supported by the grants P101/11/0207 (J. Horáček), No. 201/08/0012 (M. Feistauer, V.Kučera) of the Czech Science Foundation, and by the grants SVV-2012-265316 and GAChU 549912 financed by the Charles University in Prague (J. Hasnedlová-Prokopová and A. Kosík).

REFERENCES

[1] I. TITZE, *Principles of Voice Production.*, National Center for Voice and Speech, Iowa City, 2000.

[2] J. HORÁČEK, P. ŠIDLOF AND J. ŠVEC, *Numerical simulation of self-oscillations of human vocal folds with Hertz model of impact forces.*, J. Fluids Struct., 20 (2005), pp. 853–869.

[3] F. ALIPOUR AND I. TITZE, *Combined simulation of two-dimensional airflow and vocal fold vibration*, *Vocal fold physiology,controlling complexity and chaos*, San Diego, 1996.

[4] M. DE VRIES, H. SCHUTTE, A. VELDMAN AND G. VERKERKE, *Glottal flow through a two-mass model: comparison of Navier-Stokes solutions with simplified models.*, J. Acoust. Soc. Am., 111 (2002).

[5] P. PUNČOCHÁŘOVÁ-POŘÍZKOVÁ, K. KOZEL AND J. HORÁČEK, *Simulation of unsteady compressible flow in a channel with vibrating walls - influence of frequency.*, Computers and Fluids, 46 (2011), pp. 404–410.

[6] T. NOMURA AND T. J. R. HUGHES, *An arbitrary Lagrangian-Eulerian finite element method for interaction of flow and a rigid body.*, Comput. Methods Appl. Mech. Engrg., 95 (1992), pp. 115–138.

[7] M. FEISTAUER, J. HORÁČEK, V. KUČERA AND J. PROKOPOVÁ, *On numerical solution of compressible flow in time-dependent domains.*, Mathematica Bohemica, 137 (2011), pp. 1–16.

[8] A. KOSÍK, M. FEISTAUER, J. HORÁČEK AND P. SVÁČEK, *Numerical simulation of interaction of human vocal folds and fluid flow.*, in Vibration problems ICOVP 2011, J. Náprstek, J. Horáček, M. Okrouhlík, B. Marvalová, F. Verhulst and J. T. Sawic Georg, eds., Springer Proceedings in Physics 139 (2011), pp. 765–771.

[9] S. BADIA AND R. CODINA, *On some fluid-structure iterative algorithms using pressure segregation method. Application to aeroelasticity.*, Int. J. Numer. Meth. Engng., 172 (2007), pp. 46–71.